Nano Energy 27 (2016) 602–610

Contents lists available at ScienceDirect

Nano Energy

journal homepage: www.elsevier.com/locate/nanoen

Durable high-rate capability $Na_{0.44}MnO_2$ cathode material for sodium-ion batteries

Xin He [a], Jun Wang [a], Bao Qiu [b], Elie Paillard [c], Chuze Ma [d], Xia Cao [a], Haodong Liu [d], Marian Cristian Stan [a], Haidong Liu [a], Tobias Gallash [a], Y. Shirley Meng [d,*], Jie Li [a,**]

[a] MEET Battery Research Center, Institute of Physical Chemistry, University of Muenster, Corrensstrasse 46, 48149 Muenster, Germany
[b] Ningbo Institute of Materials Technology and Engineering (NIMTE), Chinese Academy of Sciences, Ningbo, Zhejiang 315201, PR China
[c] Helmholtz-Institut Münster (IEK-12: Ionics in Energy Storage), Forschungszentrum Jülich GmbH, 52428 Jülich, Germany
[d] Laboratory of Energy Storage and Conversion, Department of NanoEngineering, University of California, La Jolla, San Diego, CA 92093, USA

ARTICLE INFO

Article history:
Received 22 April 2016
Received in revised form
4 July 2016
Accepted 17 July 2016
Available online 18 July 2016

Keywords:
Sodium-ion batteries
Cathode
Nanoplate
Rate capability
Cycling stability

ABSTRACT

Monocrystalline orthorhombic $Na_{0.44}MnO_2$ nanoplate as a potential cathode material for sodium-ion batteries has been synthesized by a template-assisted sol-gel method. It exhibits high crystallinity, pure phase and homogeneous size distribution. During the synthesis, acidic and reductive conditions are applied to limit the production of unfavorable Birnessite phase in the precursor, and colloidal polystyrene is included to avoid morphology collapse during the gel formation and particle elongation in one direction. The decompositions of polystyrene and citric acid during high temperature firing offer a reductive carbothermal condition which can suppress the formation of unidimensional particles, and limit particle growth along the [001] direction. As a consequence, the material delivers 96 mAh g^{-1} discharge capacity at 10 C (86% of 0.1 C capacity) and maintains 97.8% capacity after 100 cycles at 0.5 C. Such superior rate capability and cycling stability of this material are among the best to date, suggesting its great interest in practical applications.

1. Introduction

The urgent demand for developing a sustainable and highly efficient energy storage system has led to a great deal of interest in lithium-ion batteries (LIBs) [1–3]. However, the geographically constrained Li mineral reserves combined with the increasing demand for Li commodity chemicals, linked to the foreseen growing implementation of large-format LIBs, will surely drive its price up. LIBs might become too expensive to be applied in the rapidly developing electric vehicles or in large stationary energy storage systems. In contrast to lithium, sodium is very abundant in nature and widely available in different forms [4]. It is also expected to show similar properties to lithium, according to their proximity in the periodic table. In addition, as sodium does not alloy with Al, it would allow substituting Cu current collector at the anode for further gains in cost and weight. These advantages of sodium motivate the exploration of rechargeable sodium-ion batteries (NIBs) as a next generation energy storage system, which indeed has attracted a great research attention recently [5–7].

As a matter of fact, Na^+ ion (de-)intercalation and storage are still very challenging since the ionic radius of Na^+ (0.98 Å) is larger than that of Li^+ (0.69 Å) [8,9], which makes the accommodation of Na^+ ions in a host material difficult and often leads to severe structural degradation [10]. Thus, developing active materials with improved rate performance and long term cycling stability for NIBs represents the main research challenge. Numerous active materials have been intensively studied as candidates for NIBs cathodes, including sodium transition metal (TM) pyrophosphates [11–13] and sodium transition metal phosphates (TM: Co, Mn, Fe, Ni, Cr, and multicomponent transition metals) [14–18]. These polyanion-based structures with stable host frameworks and strong P-O covalent bonds are thermally stable [11]. Nevertheless, most of these materials exhibit inferior electrochemical performance, especially a poor rate capability, originating from low electronic conductivity and reduced mobility at phase boundaries, which limits their practical capacity values. P2-type Na_xTMO_2 are considered to be promising candidates; and these compounds are being introduced as cathode materials for NIBs due to their facile synthesis and structural stability [19–21]. Among them, $Na_{0.44}MnO_2$ ($Na_4Mn_9O_{18}$) presents interesting characteristics linked to its open structure with interconnected and large tunnels, which is able to sustain the multiple phase change that occurs during the Na^+ (de)-insertion processes [22,23]. Sauvage et al.

* Corresponding author.
** Corresponding author.
E-mail addresses: shmeng@ucsd.edu (Y.S. Meng), jie.li@uni-muenster.de (J. Li).

http://dx.doi.org/10.1016/j.nanoen.2016.07.021
2211-2855/

demonstrated reversible insertion and extraction of Na^+ ions in pure $Na_{0.44}MnO_2$ with an initial capacity of c.a. 80 mAh g^{-1} at 0.1 C [22]. However, after 50 cycles, only half of the original capacity was retained. More recently, research focused on downsizing particle, such as nanowires. The obtained $Na_{0.44}MnO_2$ exhibited improved cycling performance combined with higher capacities [10] and less than 7% capacity fading during the first 30 cycles [10]. Although the cycling performance was improved to a certain extent, the rate capability, especially at high rate still needs to be enhanced.

Considering that $Na_{0.44}MnO_2$ bi-dimensional structures (nanoplates) extending perpendicularly to Na^+ most favorable insertion pathways would allow limiting surface defects, increasing the tap density and fast Na^+ (de)insertion (as compared to unidimensional particles), designing $Na_{0.44}MnO_2$ material with this morphology is an efficient strategy to achieve enhanced rate capability and volumetric energy density. However, it is known that Birnessite nanoplates can form as an intermediate during the firing process of $Na_{0.44}MnO_2$ [24], especially in alkaline and oxidative condition. They then split into $Na_{0.44}MnO_2$ unidimensional particles upon high temperature annealing [25], while the obtaining of bi-dimensional $Na_{0.44}MnO_2$ seems to be favored by direct high temperature sintering and the use of reductive condition, perhaps as a result of avoiding Birnessite intermediate structure. More recently, Xu et al. [26] synthesized $Na_{0.44}MnO_2$ submicron slabs by a citric acid-based sol-gel synthesis, and obtained slightly extended (001) surface. However, the obtained slabs presented in wide range of widths and several grooves collapsing on their surface, reminiscent of Birnessite splitting mechanism.

Thus, in order to avoid extensive elongation in one direction and obtain homogenous morphology, a novel sol-gel method (NSG) with self-made in-house polystyrene (PS) is applied to synthesize $Na_{0.44}MnO_2$ material in this work. PS colloidal suspension is added to the precursor solution. It serves as a dispersion additive which can avoid the collapse of morphology during the gel formation, provides extra carbon source and offers a carbothermal reductive environment during firing. Orthorhombic $Na_{0.44}MnO_2$ nanoplates are obtained, and its performance as cathode material for rechargeable NIBs is evaluated as well. In comparison, $Na_{0.44}MnO_2$ material is also synthesized by the conventional sol-gel method (SG).

2. Experimental

2.1. Synthesis

Polystyrene (PS)-contained solution was synthesized by an emulsion polymerization method. Potassium persulfate (0.12 g) and sodium dodecyl sulfate (SDS 0.4 g) were dissolved in aqueous alcohol, and then drop 40 ml of styrene monomer under Ar atmosphere and continuous rapid stirring. The colloidal suspension with dispersed PS was obtained by continuously stirring the mixture at 70 °C for 8 h.

In syntheses of $Na_{0.44}MnO_2$ active materials, stoichiometric amounts (calculated based on the 0.04 mol target material) of sodium nitrate ($NaNO_3$, Sigma-Aldrich AR), manganese acetate ($Mn(AC)_2 \cdot 4H_2O$, Sigma-Aldrich AR), as-prepared 10 ml PS-contained solution and 4 g citric acid ($C_6H_8O_7$, Sigma-Aldrich AR) were dissolved in 100 ml distilled water. Here, additional to the chelating function, citric acid provided a reductive environment. After stirring for half hour, the mixture was heated to 120 °C until all the solvent evaporated. More citric acid was added in this process to maintain the pH value in the range of 4-5, which can contribute to the homogeneous distribution of the metal precursor. The xerogel was then collected and thermal treated at 800 °C for 10 h under air to obtain the target material. For the convenience, the sample prepared under this procedure is named as NSG-$Na_{0.44}MnO_2$. To synthesize $Na_{0.44}MnO_2$ by conventional sol-gel method, a solution was initially prepared by dissolving the stoichiometric amounts of sodium nitrate and manganese acetate in 100 ml distilled water. The mixed precursor was obtained by heating the prepared solution at 120 °C for 8 h. The post thermal treatment was kept same as the NSG approach, and the sample is named as SG-$Na_{0.44}MnO_2$.

2.2. Characterization

The crystal structure was characterized by X-ray diffraction (XRD) on a Bruker D8 Advance (Bruker) with Cu K_α radiation at room temperature. The patterns were recorded in the 2θ range of 10–70°. Particle morphologies were evaluated using a field-emission scanning electron microscope (Auriga) equipped with a focused ion beam (FIB) (FE-SEM, Zeiss). The detailed crystal structure was further analyzed by transmission electron microscopy (TEM, *Zeiss Libra 200 FE*) operating at 200 kV. Selected area electron diffraction (SAED) pattern was recorded by a Gatan CCD camera in a digital format. The electronic conductivity of prepared SG-$Na_{0.44}MnO_2$ and NSG-$Na_{0.44}MnO_2$ samples were investigated by an impedance spectroscopy with Novocontrol AN-alpha analyzer and POT/GAL 20/11 electrochemical test station. Each sample was pressed under the same pressure to obtain a pellet with 1.0 mm in thickness and 8 mm in diameter. Before the conductivity measurement, both sides of pellet were coated with 120 nm thick Au. During the investigation process, an alternating current (frequency range from 100 mHz to 10 MHz) with voltage of 1 V was utilized at room temperature.

2.3. Electrochemical measurements

The slurry for preparing the cathode electrodes was obtained by mixing the active material, conductive carbon (Super C65, Imerys) and binder Poly (vinylidene fluoride) (PVdF, Kynar® FLEX 2801, Arkema Group) in a weight ratio of 80:10:10 in N-methyl-2-pyrrolidone (NMP, Sigma-Aldrich) using a ball milling method. The slurry was coated on an Al foil and dried at 80 °C overnight. After being punched into ⌀ 12 mm disc, the electrodes were further dried for 12 h under vacuum at 110 °C. The mass loading of prepared electrode is around 2 mg cm^{-2}. The electrochemical performance was evaluated in 2032 coin cells, using sodium metal foil as counter electrode. Cathode and sodium metal were separated by glass fiber mats (Whatman GF/D) wetted with 1 M sodium perchlorate ($NaClO_4$, Sigma-Aldrich) in an ethylene carbonate (EC)/propylene carbonate (PC) equivolumic mixture. Galvanostatic cycling was carried out on MACCOR series 4000 battery testers in a voltage range of 2.0– 4.0 V at various current rates. All voltages reported in this work refer to the Na counter electrode. Cyclic Voltammetry measurements were conducted on a VSP electrochemical workstation (Bio-logic), applying a sweep rate of 0.02 mV s^{-1}.

2.4. In-situ XRD measurement

In-situ XRD analysis on $Na_{0.44}MnO_2$ cathode during Na ion insertion and extraction has been performed using a cell, as being reported in our previous work [27,28]. The cell body was made of stainless steel covered internally by a Mylar foil for electrical insulation. The electrode slurry was cast directly on a glassy carbon SIGRADUR® window (180 μm, HTW Hochtemperatur Werkstoffe GmbH), which served both as current collector and “transparent window” for the X-ray beam. The coated glassy carbon was subsequently dried at 80 °C for 4 h and at 40 °C under vacuum

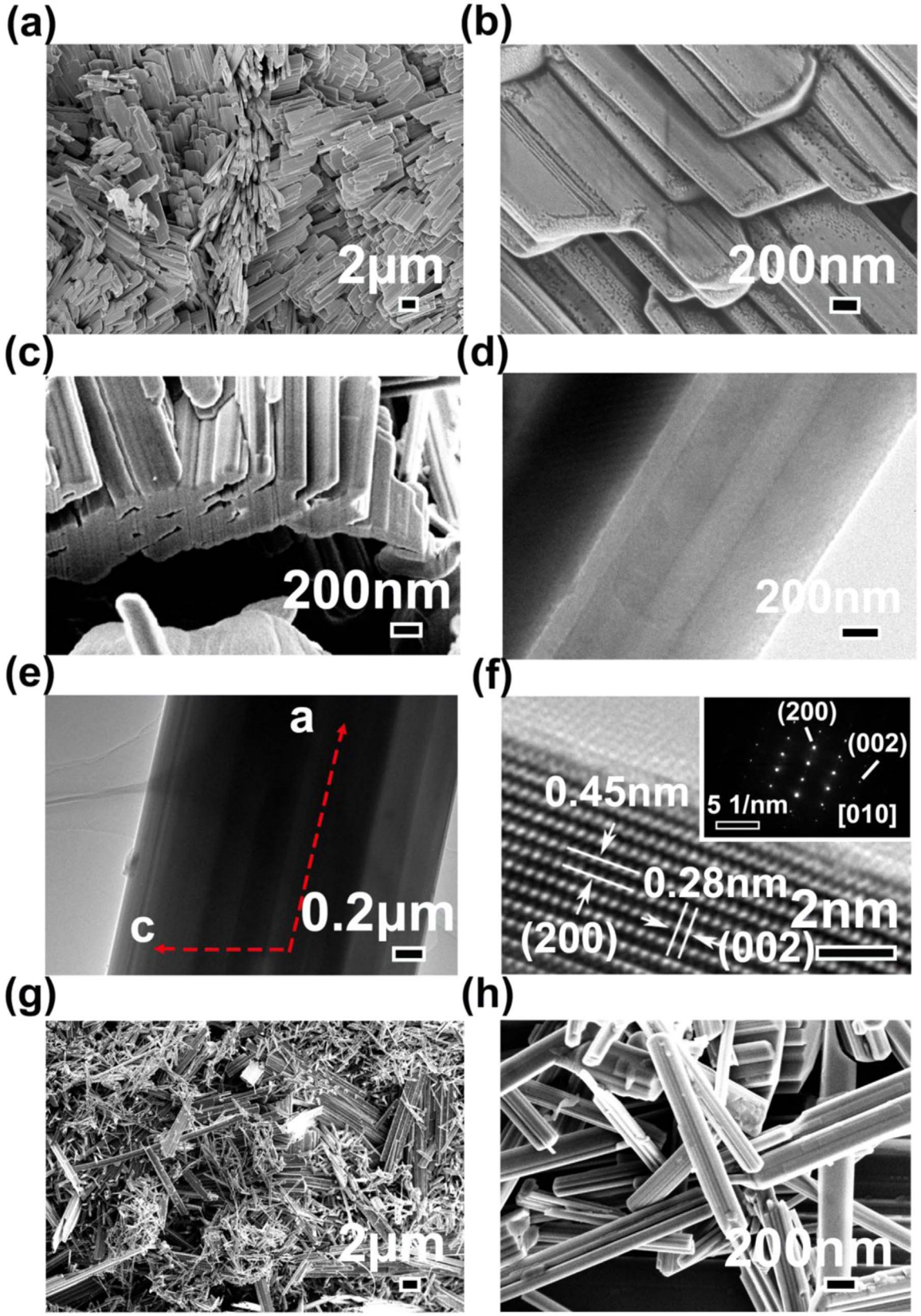

Fig. 1. SEM micrographs at the magnifications of (a) 2k ×, (b) 50k × and (c) FIB-SEM micrograph for the prepared NSG-$Na_{0.44}MnO_2$ material. (d) TEM image of an individual NSG-$Na_{0.44}MnO_2$ particle. (e) HRTEM image and (f) SAED pattern of a monocrystalline $Na_{0.44}MnO_2$ nanoplate. SEM micrographs of the SG-$Na_{0.44}MnO_2$ material under the magnifications of (g) 2k × and (h) 50k ×.

overnight. Metallic sodium foil served as counter electrode and Whatman GF/D glass fiber mats served as separators, drenched with 300 μl of electrolyte. The assembled cells were rested for 6 h before the measurement. A blank measurement of pure PVdF was carried out to confirm that the binder does not show any reflection within the investigated 2θ range. Subsequently, the cell was charged and discharged by cyclic voltammetry applying a sweep rate of 0.02 mV s^{-1} between 2.0 and 4.0 V starting from open circuit voltage (OVC) in the anodic direction (charge). In parallel, XRD analysis was performed, within the 2θ range of $10-90^{\circ}$, with a step size of 0.01838° and a step time of 0.52 s, resulting in a complete individual measurement in 40 min, with a rest period of 140 s.

3. Results and discussion

Fig. 1a and b show the SEM images of the as prepared NSG-$Na_{0.44}MnO_2$ material under different magnifications. The low magnification image (2k ×, Fig. 1a) shows a rather uniform size distribution of the particles (6 μm in length and 2 μm in width), compared with SG-$Na_{0.44}MnO_2$, as can be seen in Fig. 1g. Different from SG-$Na_{0.44}MnO_2$ (Fig. 1h), which shows more or less nanorod shape, the high magnification image (50k ×, Fig. 1b) indicates that an individual particle of NSG-$Na_{0.44}MnO_2$ is formed by several nanoplates bundled together. According to FIB image, showed in Fig. 1c, NSG-$Na_{0.44}MnO_2$ nanoplates have a specific lamellar with channels distributed between plates. The thin nanoplate (with the thickness of less than 100 nm) provides a large surface area and the channels improve the electrode/electrolyte contact. Both of them can facilitate the (de-) intercalation of Na^+-ions, enhance the Coulombic efficiency of the material and reduce the electrode polarization. More interestingly, an inner lamellar structure was also confirmed by TEM (Fig. 1d). It can be observed that the slab-like shape particle consists of a series of adherent nanoflakes overlaying each other; these nanoflakes are in the wideness of 5–20 nm, forming very well lamellar structure. The result reveals that further crystallization happens during the heating process. However, no nanowire splits from the formed stable structure, which is different as literature reported [10,25]. High resolution TEM (HRTEM) images of an individual particle (Fig. 1e and f) show (200) and (002) planes of the crystalline phase of NSG-$Na_{0.44}MnO_2$, as being labeled in Fig. 1f. The corresponding selected area electron diffraction (SAED) pattern recorded along [010] direction (insert of Fig. 1f) also displays (200) and (002) planes of NSG-$Na_{0.44}MnO_2$. Thus, the crystal grows in parallel with (010) plane, resulting in the formation of nanoplates.

It has been reported that, if the ratio of Na to Mn in the starting material is slightly higher than 0.51, a mixture of orthorhombic $Na_{0.44}MnO_2$ and hexagonal $Na_{0.7}MnO_2$ could be obtained [29]. Therefore, in order to get the pure phase, the ratio of Na and Mn agents needs to be well controlled during synthesis. The XRD patterns, as showed in Fig. 2a, confirm that the two materials obtained in this work are well consistent with the orthorhombic $Na_{0.44}MnO_2$ phase (*Pbam* space group, JCPDS no. 27-0750). There is no trace of impurities viewed in the patterns, such as Mn_2O_3, which was detected in earlier reports [30,31], or Na_xMnO_2 with x value different from 0.44. The ICP-OES determined that the mole ratio of sodium and manganese of NSG-$Na_{0.44}MnO_2$ sample was 0.435:1, within the 2% error of the expected 0.44:1. The crystallinity of NSG-$Na_{0.44}MnO_2$ is much better than that of SG-$Na_{0.44}MnO_2$ due to the relatively narrow and high diffraction peaks. The schematic illustration, in Fig. 2b (right), shows that the crystal structure of $Na_{0.44}MnO_2$ includes two groups of manganese ion units: sheets of edge-sharing octahedra MnO_6 which consists of all Mn^{4+} ions and half of the Mn^{3+}, and columns of square-pyramids MnO_5 built by the rest Mn^{3+}. Two types of complex tunnels can be built from the different edge-linked chains. Na_1 and Na_2 sites are situated in large S-shaped tunnels, while Na_3 site is located in smaller pentagonal tunnels [32,33]. The main diffusion pathway for Na^+ ions is along the c-axis ([001] direction). When the material is fully discharged, all the sodium sites are occupied with the formula of $Na_{0.66}MnO_2$ [22,34]. The wide tunnel structure may accommodate the stresses associated with the structure change during electrochemical process and benefit the cycling performance. Therefore, the rate capability of NIBs employing $Na_{0.44}MnO_2$ as cathode materials can be significantly improved by tuning the crystal habit.

Fig. 3a illustrates the crystal growth of NSG-$Na_{0.44}MnO_2$ material, which is concluded from TEM and XRD results. The *c* axis, which is also the crystal orientation [001], has been reported as the favorite direction of the crystal growth for $Na_{0.44}MnO_2$ [35–37]. As the result, the nanorod shape for this material is preferred, and relatively lower amount of (001) planes on the particle surface is obtained. It is also proved by SG-$Na_{0.44}MnO_2$ synthesized in this work, the material crystalizes into rod-shape particles as showed in Fig. 1h. Since it is also the direction of large S-shape channel for Na^+ (de)-insertion [26], the long distance of Na^+ diffusion pathway as well as the limited rate performance of the material unfortunately can be expected. Different from the nanorod, the crystal of nanoplate shape grows in parallel with (010) plane, which can not only limit the length of the crystal structure along *c* axis ([001] direction), but also increase the length along *a* axis ([100] direction). Thus, the particle surface perpendicular to *c* axis is enlarged and the better rate capability will be achieved. Meanwhile, as being showed in Fig. 3b, the relatively thin nanoflake and tunnel among the overlapping nanoflakes could reduce the diffusion distance of Na^+ ions and benefit the electrolyte permeation. With these advantages, a great enhancement of electrochemical performance can be expected from the as prepared NSG-$Na_{0.44}MnO_2$ nanoplates.

The electrochemical behaviors of the NSG-$Na_{0.44}MnO_2$ were first

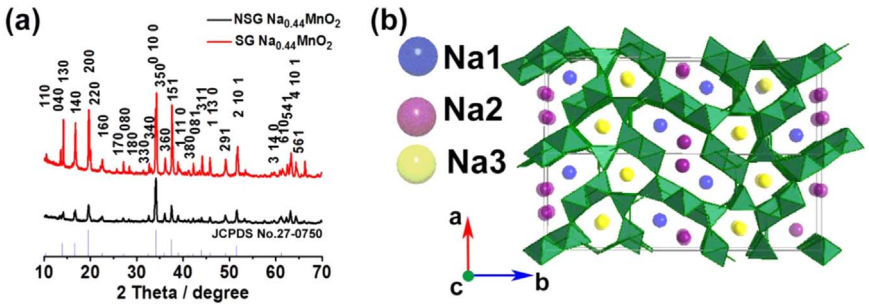

Fig. 2. XRD patterns of SG-$Na_{0.44}MnO_2$ and NSG-$Na_{0.44}MnO_2$ samples (a) and corresponding structure schematic illustration (b) of the orthorhombic $Na_{0.44}MnO_2$ in the *Pbam* space group (view perpendicular to the ab plane).

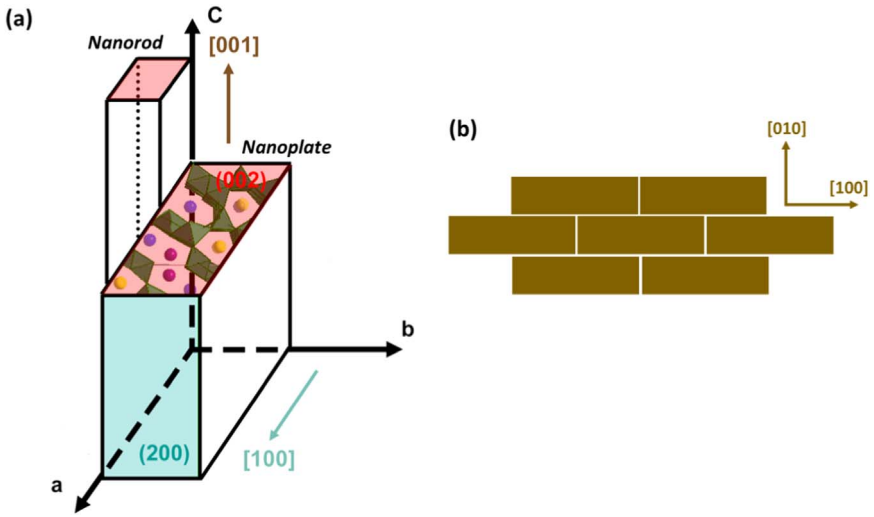

Fig. 3. Schematic illustration for crystal growth of nanorod and nanoplate (a); the structural formation of nanoplate particles (b).

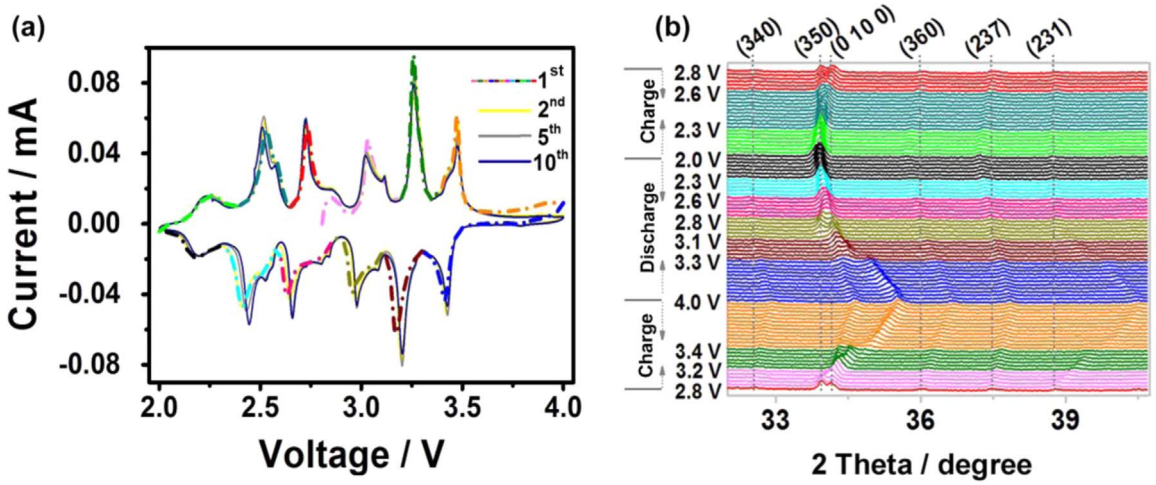

Fig. 4. Cyclic voltammogramms of (a) NSG-$Na_{0.44}MnO_2$ electrode between 2.0 and 4.0 V at a potential sweep rate of 0.1 mV s^{-1}. *In situ* evolution of the XRD pattern (b) recorded at 0.02 mV s^{-1} voltage sweep rate of NSG-$Na_{0.44}MnO_2$ between 2.0 and 4.0 V.

investigated by cyclic voltammetry (CV) with a sweep rate of 0.02 mV s^{-1} between 2.0 and 4.0 V. The resulting voltammograms are shown in Fig. 4a. The first cycle exhibits at least six pairs of symmetrical redox peaks, which represent the different intercalation/deintercalation steps of Na^+ ions into/from NSG-$Na_{0.44}MnO_2$, presented by different colors of the first CV plot (Fig. 4a). The redox peaks were attributed to consecutive two-phase reaction mechanism [10,22,38], but the highly reproduced shape and the very small voltage gap between each redox couple imply the fast diffusion of Na^+ ions during the electrochemical measurement. Nevertheless, a weak oxidation peak (when the voltage is higher than 3.6 V) in the initial anodic scan has no corresponding reductive peak, which may be attributed to the electrolyte decompositions. Except this, the shape of the oxidation/reduction peaks after the first cycle remains unchanged, indicating an excellent reversibility of Na insertion into NSG-$Na_{0.44}MnO_2$.

In order to investigate the initial electrochemical reaction of NSG-$Na_{0.44}MnO_2$, *in-situ* XRD analysis coupled with electrochemical process has been performed using an *in-house* designed cell. The XRD patterns obtained during the first oxidation/reduction process of the Na/$Na_{0.44}MnO_2$ cell in the restricted 2θ degree region from 32 to 40° are displayed in Fig. 4b. The diffraction patterns are structurally close associated with the voltage plateaus from the beginning of Na extraction process, and each step is distinguished by different colors in relation to the initial curve of the CV measurement (Fig. 4a). During the first charge process, most of the diffraction peaks of NSG-$Na_{0.44}MnO_2$ shift to higher 2θ angle, indicating that the extraction of Na^+ ions from the structure would lead to the decrease of the lattice parameters. The peak changes due to the two-phase reaction. During the following discharge process, the diffraction peaks shift back in a very symmetrical way. The peaks of the same voltage, for both charge and discharge, locate in the same 2θ position with little change in intensity. It is interesting to see that the peaks for the planes which are perpendicular, such as (0 10 0), and are nearly perpendicular, such as (1 11 0), to *b* axis, show obviously bigger shift than the others. This means that the expansion and contraction of the lattice during the Na extraction / insertion are along the *b* axis. All these appearances indicate a highly reversible process of the extraction/insertion of Na^+ ions. Based on the *in-situ* XRD results, the charge/discharge process does not lead to any new phases, and NSG-$Na_{0.44}MnO_2$ cathode material has excellent reversibility, which proves again the conclusions from the CV measurement.

Considering the detrimental impact of the specific particle morphologies on the high rate discharge and capacity retention, we have investigated the rate and long-term cycling performances of the synthesized material. The discharge rate capability of the two $Na_{0.44}MnO_2$ cathodes is shown in Fig. 5a. The cells were cycled at

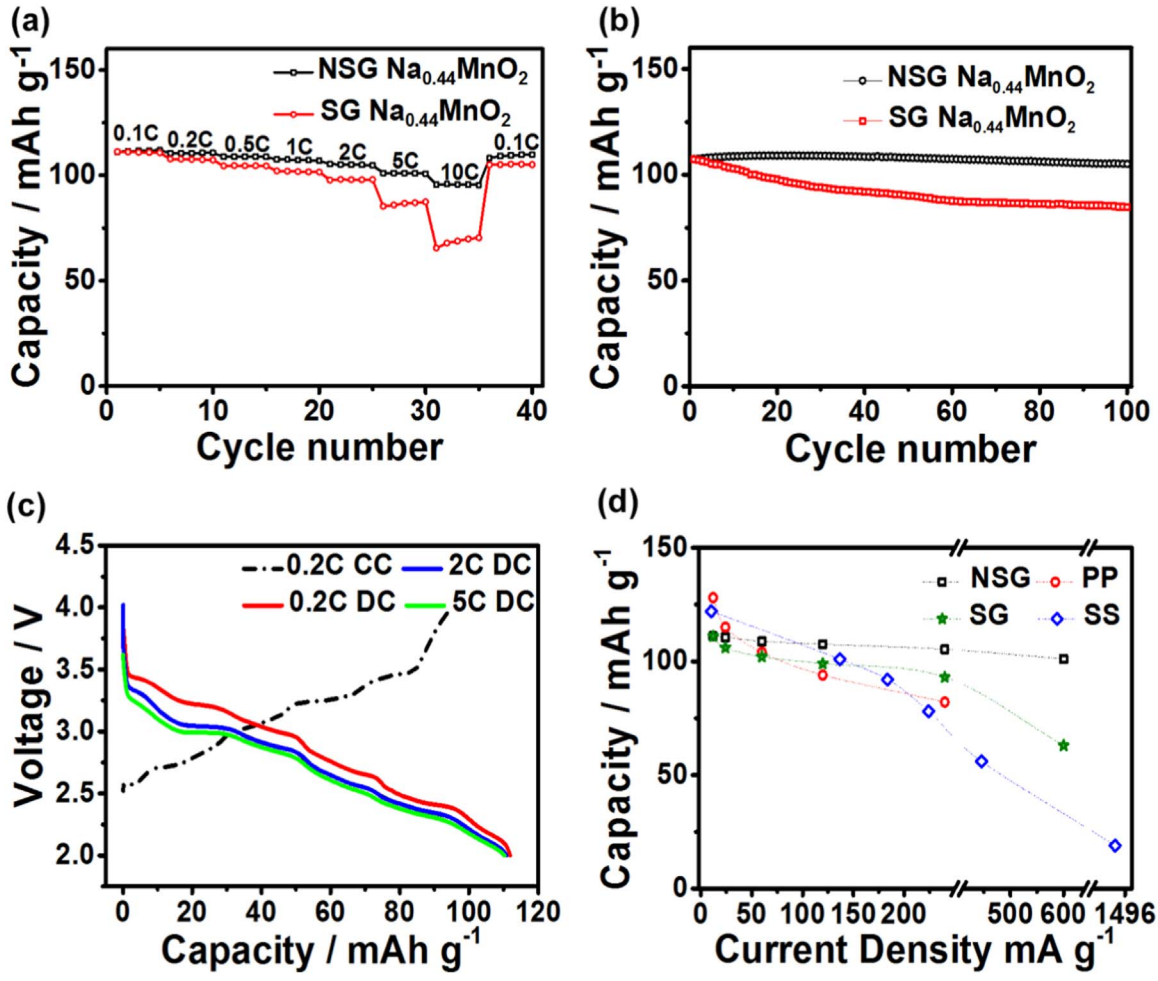

Fig. 5. (a) Rate capabilities of the as-prepared SG-$Na_{0.44}MnO_2$ and NSG-$Na_{0.44}MnO_2$ nanoplates. (b) Cycling behaviors of the SG-$Na_{0.44}MnO_2$ and NSG-$Na_{0.44}MnO_2$ nanoplates at 0.5 C for 100 cycles. (c) The discharge profiles of NSG-$Na_{0.44}MnO_2$ at 0.2, 2 and 5 C (The charge current rate is fixed at 0.2 C). (d) Comparison in the rate performance of the NSG-$Na_{0.44}MnO_2$ with the literature reports for the same materials prepared by solid state reactions (SS) [22,41], sol-gel routes (SG) [29,42] and polymer-pyrolysis (PP) method [10].

various charge and discharge rates ranging from 0.1 to 10 C (1 C is defined as 120 mA g^{-1}) in a voltage range of 2.0–4.0 V. It can be observed that NSG-$Na_{0.44}MnO_2$ exhibits much better rate performance than SG-$Na_{0.44}MnO_2$, especially at high rate. Specially, NSG-$Na_{0.44}MnO_2$ delivers a discharge capacity of 96 mAh g^{-1} at current density 10 C, which is actually 86% of the capacity (112 mAh g^{-1}) at 0.1 C. Strikingly, a capacity of about 112 mAh g^{-1}, same as the initial capacity, can be recovered when the current density returns to 0.1 C after the high rates test. These results suggest that NSG-$Na_{0.44}MnO_2$ electrode can fully afford rapid charge and discharge. Generally, Na^+ ions insertion into and extraction from oxide hosts are considered with poor kinetics, compared with their Li-ion analogues due to the much larger size of Na^+ ions than Li^+ ions and 1D diffusion pathway of Na^+ ions for the orthorhombic $Na_{0.44}MnO_2$, but this is not the case of the material synthesized in this work. The good rate capability of the NSG-$Na_{0.44}MnO_2$ electrode was also confirmed by electronic conductivity measurement. The bulk electronic conductivity of NSG- $Na_{0.44}MnO_2$ sample is 7.7×10^{-5} S cm^{-1} which has improved around one or two orders of magnitude comparing to the result of SG-$Na_{0.44}MnO_2$ sample (5×10^{-6} S cm^{-1}). In summary, the relatively high rate capability is related to the pure phase, stabilized structure, improved electronic conductivity, well controlled morphology with limited crystal growth along the [001] direction and less polarization of the $a_{0.44}MnO_2$ material obtained by the NSG method, as indicated by structure, morphology characterizations, conductivity measurement and CV analysis. The cycling stability of the two $Na_{0.44}MnO_2$ cathodes are tested under the current rate of 0.5 C, and the results are showed in Fig. 5b. Superior to SG-$Na_{0.44}MnO_2$, which maintains 78.9% initial capacity after 100 cycles, NSG-$Na_{0.44}MnO_2$ presents excellent capacity retention, with no more than 2.2% capacity loss after 100 cycles (from 108 mAh g^{-1} in the first cycle decreases to 105 mAh g^{-1} in the 100th cycle), almost unnoticeable for the plot. The slight 3 mAh g^{-1} capacity decrease may be ascribed to the electrolyte degradation, or the strain caused by Jahn-Teller distortion and the structure degradation upon cycling [38]. Further study is needed to fully understand these subtle yet critical phenomena. Nevertheless, it is obvious that the sodium (de)-intercalation in NSG-$Na_{0.44}MnO_2$ shows much better reversibility than SG-$Na_{0.44}MnO_2$. The better crystallinity and homogenous particle morphology could be responsible for that.

The initial different discharge profiles of the NSG-$Na_{0.44}MnO_2$ electrodes were shown in Fig. 5c. The data were obtained by testing the electrodes at the same charge current density of 0.2 C, but discharged at 0.2, 2 and 5 C, respectively. It delivers reversible discharge capacities of 112, 111 and 110 mAh g^{-1}, respectively. Agree with the CV plots, six voltage plateaus can be viewed. With increasing the discharge current density, the material still retains high capacities, although the discharge voltage profiles slightly

shift to lower voltage. This behavior can affect the energy density of the NIBs using $Na_{0.44}MnO_2$ as active material. However, no obvious voltage decay is found when the current density changes from 2 to 5 C. Compared the rate capability of NSG-$Na_{0.44}MnO_2$ (based on Fig. 5a) with the literature reported $Na_{0.44}MnO_2$ materials (Fig. 5d) synthesized by solid state reactions (SS), sol-gel routes (SG), polymer-pyrolysis (PP) methods [10,22,25,29,39–42], our results are evidently encouraging. To the best of our knowledge, this material exhibits by far the best performance in the case of high rate capability and excellent cycling stability for Na^+-ions storage. The high discharge capacity and power density, significant high rate capability and the low cost of the $Na_{0.44}MnO_2$ nanoplate make it practically applicable in large power devices and EVs.

4. Conclusions

In summary, the pure monocrystal $Na_{0.44}MnO_2$ nanoplate was synthesized by the template-assisted sol-gel method and applied as cathodes for sodium ion batteries. The material shows high crystallinity and homogeneous nanoplate morphology. The lamellar structure $Na_{0.44}MnO_2$ material, owning to well distributed channels and controlled morphology with limited crystal growth along [001] direction, can provide a mechanically stable construction corresponded with short diffusion path for Na^+ ions insertion/extraction. Electrochemical performance revealed the obtained $Na_{0.44}MnO_2$ nanoplates exhibited excellent reversibility, outstanding high rate capability (96 mAh g^{-1} at 10 C) and remarkable cycling stability (less than 2.2% loss in 100 cycles at 0.5 C), which are much better than other previously reported $Na_{0.44}MnO_2$ compounds in the term of capability and cycling stability. The as-prepared $Na_{0.44}MnO_2$ nanoplates represent a promising cathode material for high power NIBs.

Acknowledgments

The authors kindly acknowledge the financial support of the Federal Ministry of Education and Research (BMBF), the Federal Ministry of Economic and Technology (BMWi) and the Federal Ministry for the Environment, Nature Conservation and Nuclear Safety (BMU) of Germany within the project KaLiPat (G.A. no. 03EK3008). E. Paillard acknowledges the funding of the 'SPICY' project within the 'Horizon 2020' program (G.A. no. 653373) of the European Commission. C.Z. Ma, H.D. Liu and Y.S. Meng (UCSD) acknowledge the funding support by National Science Foundation under award number DMR1057170.

References

[1] M.M. Thackeray, C. Wolverton, E.D. Isaacs, Electrical energy storage for transportation-approaching the limits of, and going beyond, lithium-ion batteries, Energy Environ. Sci. 5 (2012) 7854–7863.
[2] B. Dunn, H. Kamath, J.-M. Tarascon, Electrical energy storage for the grid: a battery of choices, Science 334 (2011) 928–935.
[3] Y. Gogotsi, P. Simon, True performance metrics in electrochemical energy storage, Science 334 (2011) 917–918.
[4] B.L. Ellis, L.F. Nazar, Sodium and sodium-ion energy storage batteries, Curr. Opin. Solid State Mater. Sci. 16 (2012) 168–177.
[5] S.-W. Kim, D.-H. Seo, X. Ma, G. Ceder, K. Kang, Electrode materials for rechargeable sodium-ion batteries: potential alternatives to current lithium-ion batteries, Adv. Energy Mater. 2 (2012) 710–721.
[6] V. Palomares, P. Serras, I. Villaluenga, K.B. Hueso, J. Carretero-Gonzalez, T. Rojo, Na-ion batteries, recent advances and present challenges to become low cost energy storage systems, Energy Environ. Sci. 5 (2012) 5884–5901.
[7] M.D. Slater, D. Kim, E. Lee, C.S. Johnson, Sodium-ion batteries, Adv. Funct. Mater. 23 (2013) 947–958.
[8] S. Li, Y. Dong, L. Xu, X. Xu, L. He, L. Mai, Effect of carbon matrix dimensions on the electrochemical properties of $Na_3V_2(PO_4)_3$ nanograins for high-performance symmetric sodium-ion batteries, Adv. Mater. 26 (2014) 3545–3553.
[9] S.Y. Hong, Y. Kim, Y. Park, A. Choi, N.-S. Choi, K.T. Lee, Charge carriers in rechargeable batteries: Na ions vs. Li ions, Energy Environ. Sci. 6 (2013) 2067–2081.
[10] Y. Cao, L. Xiao, W. Wang, D. Choi, Z. Nie, J. Yu, L.V. Saraf, Z. Yang, J. Liu, Reversible sodium ion insertion in single crystalline manganese oxide nanowires with long cycle life, Adv. Mater. 23 (2011) 3155–3160.
[11] H. Kim, R.A. Shakoor, C. Park, S.Y. Lim, J.-S. Kim, Y.N. Jo, W. Cho, K. Miyasaka, R. Kahraman, Y. Jung, J.W. Choi, $Na_2FeP_2O_7$ as a promising iron-based pyrophosphate cathode for sodium rechargeable batteries: a combined experimental and theoretical study, Adv. Funct. Mater. 23 (2013) 1147–1155.
[12] P. Barpanda, G. Liu, C.D. Ling, M. Tamaru, M. Avdeev, S.-C. Chung, Y. Yamada, A. Yamada, $Na_2FeP_2O_7$: a safe cathode for rechargeable sodium-ion batteries, Chem. Mater. 25 (2013) 3480–3487.
[13] C.S. Park, H. Kim, R.A. Shakoor, E. Yang, S.Y. Lim, R. Kahraman, Y. Jung, J. W. Choi, Anomalous manganese activation of a pyrophosphate cathode in sodium ion batteries: a combined experimental and theoretical study, J. Am. Chem. Soc. 135 (2013) 2787–2792.
[14] Z. Jian, W. Han, X. Lu, H. Yang, Y.-S. Hu, J. Zhou, Z. Zhou, J. Li, W. Chen, D. Chen, L. Chen, Superior electrochemical performance and storage mechanism of $Na_3V_2(PO_4)_3$ cathode for room-temperature sodium-ion batteries, Adv. Energy Mater. 3 (2013) 156–160.
[15] M. Casas-Cabanas, V.V. Roddatis, D. Saurel, P. Kubiak, J. Carretero-Gonzalez, V. Palomares, P. Serras, T. Rojo, Crystal chemistry of Na insertion/deinsertion in $FePO_4$-$NaFePO_4$, J. Mater. Chem. 22 (2012) 17421–17423.
[16] P. Moreau, D. Guyomard, J. Gaubicher, F. Boucher, Structure and stability of sodium intercalated phases in olivine $FePO_4$, Chem. Mater. 22 (2010) 4126–4128.
[17] K.T. Lee, T.N. Ramesh, F. Nan, G. Botton, L.F. Nazar, Topochemical synthesis of sodium metal phosphate olivines for sodium-ion batteries, Chem. Mater. 23 (2011) 3593–3600.
[18] S.Y. Lim, H. Kim, J. Chung, J.H. Lee, B.G. Kim, J.-J. Choi, K.Y. Chung, W. Cho, S.-J. Kim, W.A. Goddard, Y. Jung, J.W. Choi, Role of intermediate phase for stable cycling of $Na_7V_4(P_2O_7)_4PO_4$ in sodium ion battery, Proc. Natl. Acad. Sci. 111 (2014) 599–604.
[19] S.-M. Oh, S.-T. Myung, C.S. Yoon, J. Lu, J. Hassoun, B. Scrosati, K. Amine, Y.-K. Sun, Advanced Na[Ni0.25Fe0.5Mn0.25]O_2/C–Fe_3O_4 sodium-ion batteries using EMS electrolyte for energy storage, Nano Lett. 14 (2014) 1620–1626.
[20] N. Yabuuchi, M. Kajiyama, J. Iwatate, H. Nishikawa, S. Hitomi, R. Okuyama, R. Usui, Y. Yamada, S. Komaba, P2-type Nax[Fe1/2Mn1/2]O_2 made from earth-abundant elements for rechargeable Na batteries, Nat. Mater. 11 (2012) 512–517.
[21] R. Berthelot, D. Carlier, C. Delmas, Electrochemical investigation of the P_2–Na_xCoO_2 phase diagram, Nat. Mater. 10 (2011) 74–80.
[22] F. Sauvage, L. Laffont, J.M. Tarascon, E. Baudrin, Study of the insertion/deinsertion mechanism of sodium into Na0.44MnO_2, Inorg. Chem. 46 (2007) 3289–3294.
[23] A. Caballero, L. Hernan, J. Morales, L. Sanchez, J. Santos Pena, M.A.G. Aranda, Synthesis and characterization of high-temperature hexagonal P_2-Na0.6 MnO_2 and its electrochemical behaviour as cathode in sodium cells, J. Mater. Chem. 12 (2002) 1142–1147.
[24] P. Le Goff, N. Baffier, S. Bach, J.P. Pereira-Ramos, R. Messina, Structural and electrochemical characteristics of a lamellar sodium manganese oxide synthesized via a sol-gel process, Solid State Ion. 61 (1993) 309–315.
[25] Y. Li, Y. Wu, Formation of Na0.44MnO_2 nanowires via stress-induced splitting of birnessite nanosheets, Nano Res. 2 (2009) 54–60.
[26] M. Xu, Y. Niu, C. Chen, J. Song, S. Bao, C.M. Li, Synthesis and application of ultra-long Na0.44MnO2 submicron slabs as a cathode material for na-ion batteries, RSC Adv. 4 (2014) 38140–38143.
[27] D. Bresser, E. Paillard, R. Kloepsch, S. Krueger, M. Fiedler, R. Schmitz, D. Baither, M. Winter, S. Passerini, Carbon coated $ZnFe_2O_4$ nanoparticles for advanced lithium-ion anodes, Adv. Energy Mater. 3 (2013) 513–523.
[28] J. Wang, X. He, D. Zhou, F. Schappacher, X. Zhang, H. Liu, M.C. Stan, X. Cao, R. Kloepsch, M.S. Sofy, G. Schumacher, J. Li, O_3-type Na[Fe1/3Ni1/3Ti1/3]O_2 cathode material for rechargeable sodium ion batteries, J. Mater. Chem. A 4 (2016) 3431–3437.
[29] X. Zhou, R.K. Guduru, P. Mohanty, Synthesis and characterization of Na0.44MnO_2 from solution precursors, J. Mater. Chem. A 1 (2013) 2757–2761.
[30] A.D. Tevar, J.F. Whitacre, Relating synthesis conditions and electrochemical performance for the sodium intercalation compound $Na_4Mn_9O_{18}$ in aqueous electrolyte, J. Electrochem. Soc. 157 (2010) A870–A875.
[31] M.M. Doeff, A. Anapolsky, L. Edman, T.J. Richardson, L.C. De Jonghe, A high-rate manganese oxide for rechargeable lithium battery applications, J. Electrochem. Soc. 148 (2001) A230–A236.
[32] I. Kruk, P. Zajdel, W. van Beek, I. Bakaimi, A. Lappas, C. Stock, M.A. Green, Coupled commensurate cation and charge modulation in the tunneled structure, Na0.40(2)MnO_2, J. Am. Chem. Soc. 133 (2011) 13950–13956.
[33] J.A. Saint, M.M. Doeff, J. Wilcox, Electrode materials with the Na0.44MnO_2 structure: effect of titanium substitution on physical and electrochemical properties, Chem. Mater. 20 (2008) 3404–3411.
[34] M.M. Doeff, M.Y. Peng, Y. Ma, L.C. De Jonghe, Orthorhombic Na_x MnO_2 as a cathode material for secondary sodium and lithium polymer batteries, J. Electrochem. Soc. 141 (1994) L145–L147.
[35] C. Liu, J. Li, P. Zhao, W. Guo, X. Yang, Fast preparation of Na0.44MnO_2 nanorods

via a high NaOH concentration hydrothermal soft chemical reaction and their lithium storage properties, J. Nanopart. Res. 17 (2015) 1–8.
[36] P. Zhan, S. Wang, Y. Yuan, K. Jiao, S. Jiao, Facile synthesis of nanorod-like single crystalline $Na0.44MnO_2$ for high performance sodium-ion batteries, J. Electrochem. Soc. 162 (2015) A1028–A1032.
[37] S. Demirel, E. Oz, E. Altin, S. Altin, A. Bayri, P. Kaya, S. Turan, S. Avci, Growth mechanism and magnetic and electrochemical properties of $Na0.44MnO_2$ nanorods as cathode material for Na-ion batteries, Mater. Charact. 105 (2015) 104–112.
[38] H. Kim, D.J. Kim, D.-H. Seo, M.S. Yeom, K. Kang, D.K. Kim, Y. Jung, Ab initio study of the sodium intercalation and intermediate phases in $Na0.44MnO_2$ for sodium-ion battery, Chem. Mater. 24 (2012) 1205–1211.
[39] M.M. Doeff, T.J. Richardson, J. Hollingsworth, C.-W. Yuan, M. Gonzales, Synthesis and characterization of a copper-substituted manganese oxide with the $Na0.44MnO_2$ structure, J. Power Sources 112 (2002) 294–297.
[40] E. Hosono, T. Saito, J. Hoshino, M. Okubo, Y. Saito, D. Nishio-Hamane, T. Kudo, H. Zhou, High power Na-ion rechargeable battery with single-crystalline $Na0.44MnO_2$ nanowire electrode, J. Power Sources 217 (2012) 43–46.
[41] L. Zhao, J. Ni, H. Wang, L. Gao, $Na0.44MnO_2$-CNT electrodes for non-aqueous sodium batteries, RSC Adv. 3 (2013) 6650–6655.
[42] D.J. Kim, R. Ponraj, A.G. Kannan, H.-W. Lee, R. Fathi, R. Ruffo, C.M. Mari, D. K. Kim, Diffusion behavior of sodium ions in $Na0.44MnO_2$ in aqueous and non-aqueous electrolytes, J. Power Sources 244 (2013) 758–763.

Xin He received his bachelor degree in Polymer Materials and Engineering, East China University of Science and Technology, China. In 2012, he obtained his Master in Material Science and Engineering, Lulea Technology University, Sweden. Now he is a pH. D candidate in MEET Battery Research Center at University of Muenster (Germany) under the supervision of Dr. Jie Li and Prof. Martin Winter. His research interests include the design, synthesis and electrochemical investigations of electrode materials for lithium/sodium-ion batteries.

Dr. Jun Wang obtained his pH. D. degree from Ningbo Institute of Materials Technology & Engineering (NIMTE), Chinese Academy of Sciences, China, in 2012. Now, he is a research associate at MEET Battery Research Center, University of Muenster. His research interest is synthesis of cathode materials for lithium-ion batteries and sodium-ion batteries.

Dr. Bao Qiu is currently research staff member at Ningbo Institute of Materials Technology and Engineering (NIMTE), Chinese Academy of Sciences. He received his pH. D. in materials physics and chemistry from University of Chinese Academy of Sciences. His main research interests include the design of lithium ion battery electrode cathode materials and their structure-electrochemical property relationships.

Dr. Elie Paillard, electrochemist, received a MS Engineering and then a MSc (INP Grenoble, France, 2003 and 2004). After a pH. D on polymer electrolytes (Grenoble, dir. Prof. J.-Y. Sanchez, 2008), he joined Prof. W. Henderson in NC State University (USA) for two years, working on ionic liquids, before joining Profs Passerini and Winter in Muenster University (MEET), where he worked on various Li-ion and Li-metal related topics (nanomaterials, binder, electrolytes, Li-air). After a stay at Helmholtz Institute Ulm (Passerini group), he joined Helmholtz Institute Muenster in March 2015 as young investigator group leader.

Chuze Ma received his bachelor degree in Materials Science and Engineering from the University of Science and Technology Beijing. He is now a pH. D candidate at the University of California San Diego, pursuing his degree in Nano-engineering. He is interested in the exploration of new electrode materials and their applications for energy storage, especially the grid storage of renewable energies.

Xia Cao earned her Master degree from State Key Laboratory of Physical Chemistry of Solid Surfaces, College of Chemistry and Chemical Engineering, Xiamen University, China, in 2013. Now she is a pH. D candidate in Electrolyte Group of Prof. Martin Winter at MEET Battery Research Center, University of Muenster. Her research interests focus on electrolyte development and fundamental understanding of electrode/electrolyte interfaces for rechargeable lithium batteries.

Haodong Liu received his BS in Chemistry from Xiamen University (2011). He is currently a PhD candidate in the Nanoengineering Department at the University of California San Diego (UCSD). He is the founder of Electrochemical Society – UCSD Student Chapter, which promotes the interest and advancement of electrochemistry science and technology among both graduate and undergraduate students at UCSD. His research objective is to diagnose, optimize and design Ni and Mn based layered oxides as cathode materials for next generation Li-ion batteries and Na-ion batteries.

Dr. Marian Cristian Stan is a research associate in the Institute of Physical Chemistry and MEET Battery Research Center. He received his pH. D degree from the Westfälische Wilhelms-Universität Münster (Germany) in 2011. The main research interests deal with the development and characterization of negative active materials for Lithium-ion (conversion type) and Lithium-metal batteries of next generation (Li-air and Li-sulfur) with a focus on lithium metal.

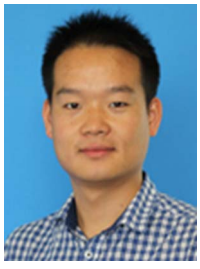

Haidong Liu received his B. S. in Chemistry (Normal) in 2009 from Changshu Institute of Technology, Suzhou and his M. S. in Physical Chemistry from Shanghai University in 2012. He is a pH. D candidate in MEET Battery Research Center at University of Muenster (Germany) under the supervision of Prof. Martin Winter and Dr. Jie Li. His research interests include the design, synthesis and electrochemical investigations of various cathode and anode materials for lithium/sodium-ion batteries.

Dr. Tobias Gallasch received his pH. D. in experimental physics from the Institute of Materials Physics, University of Muenster, Germany, in 2014. He worked on electrochemical characterization and transmission electron microscopy of sputter deposited thin film electrodes for lithium ion batteries. Currently, he holds a position as research associate in the cell technology division at MEET Battery Research Center, University of Muenster, focusing on process development and supporting the in-house pilot plant scale electrode production.

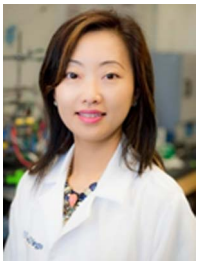

Dr Y. Shirley Meng received her PhD in Advanced Materials for Micro & Nano Systems from the Singapore-MIT Alliance in 2005. Shirley is currently the Professor of NanoEngineering, University of California San Diego (UCSD). She is the principal investigator of a research group – Laboratory for Energy Storage and Conversion (LESC) – which focuses on functional nano- and micro-scale materials for energy storage and conversion. She is the founding Director of Sustainable Power and Energy Center (SPEC), consisting of faculty members from interdisciplinary fields, aiming at making breakthroughs in distributed energy generation, storage and the accompanying power-management systems. Web: http://smeng.ucsd.edu/ and http://spec.ucsd.edu.

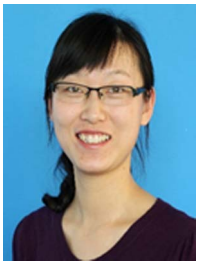

Jie Li received her PhD degree in Chemistry from Xiamen University (China) in 2008 and carried out the post-doctoral research at MEET Battery research center in University of Muenster (Germany, 2009–2012). Now, she is an independent young research group leader in MEET Battery Research Center, co-founded by three ministries in Germany (BMBF, BMWi and BMU). Her research interests focus on material synthesis, characterization and their electrochemical process for energy storage systems.